

# Restart expedites quantum walk hitting times

Ruoyu Yin<sup>1</sup> and Eli Barkai<sup>1</sup>

<sup>1</sup>*Department of Physics, Institute of Nanotechnology and Advanced Materials, Bar-Ilan University, Ramat-Gan 52900, Israel*

Classical first-passage times under restart are used in a wide variety of models, yet the quantum version of the problem still misses key concepts. We study the quantum hitting time with restart using a monitored quantum walk. The restart strategy eliminates the problem of dark states, i.e. cases where the particle evades detection, while maintaining the ballistic propagation which is important for fast search. We find profound effects of quantum oscillations on the restart problem, namely a type of instability of the mean detection time, and optimal restart times that form staircases, with sudden drops as the rate of sampling is modified. In the absence of restart and in the Zeno limit, the detection of the walker is not possible and we examine how restart overcomes this well-known problem, showing that the optimal restart time becomes insensitive to the sampling period.

*Introduction.* First-passage processes are ubiquitous in practically all fields of science. Probably the simplest approach uses a random walker in search for a target, as found for diffusion-controlled reactions [1, 2]. This common method does not demand an input of energy however it is non-efficient as the random walker resamples previously-visited locations and further the walker according to the laws of chance may stray far from the target. In the context of biochemical reactions nature found a way to overcome this problem, and that is with a restart strategy [3–6]. It turns out that sometimes, if the search does not find its target it is better to give up, and start the process anew. Restarts were employed to accelerate algorithms [7, 8], and then considered in generality in the context of stochastic processes [9, 10], rapidly encompassing various contexts including classical search theory, chemical physics and population dynamics, etc. In this well-studied field the basic questions are what are the non-equilibrium steady states emerging from restart, and what is the optimal time to restart [7–35].

As the counterpart of classical random walks, quantum walks are widely applied in many different fields, ranging from transport in waveguides to ultra-cold atoms to light-harvesting dynamics in biochemistry [36–40], and therefore rather naturally a few previous works addressed the restart problem with an underlying quantum dynamics [41–47]. At the same time, quantum search and transport, in the absence of restarts, has an antagonist: the dark subspace [48, 49], caused by destructive interference. This problem works against the quantum advantage of ballistic propagation [39], which can be useful for search. This means that for quantum walks with dark states, the detection probability, defined below, is less than unity even for small systems. Overcoming this hurdle is important for efficient quantum search and restarts are a powerful approach for that aim. However, one may not introduce restarts blindly, as the goal is not merely to get rid of the dark states, but rather to optimize the time for search. The basic questions are: How to choose the time for the restart so that the quantum search time is minimized? Will the ballistic superiority of the quantum search be retained when restart is added? What are

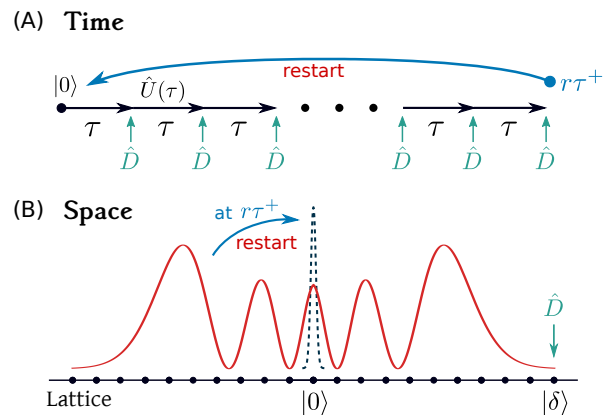


FIG. 1. The measurement protocol under sharp restart in time (A) and space (B) representation. The system is initialized at state  $|0\rangle$  [see also the dashed needle in (B)] and the unitary evolution  $\hat{U}(\tau)$  is repeatedly interrupted by projective measurements defined with  $\hat{D} = |\delta\rangle\langle\delta|$  at times  $\tau, 2\tau, 3\tau, \dots$ . If the state is detected we are done, if not at the  $r$ -th failure of detection, the system is brought back to  $|0\rangle$ , i.e. a restart is performed every  $r$  steps. The red curve in (B) represents the wave packet, namely the solution of Eq. (2), that spreads out ballistically before the particle is detected or reset.

the fundamental differences between quantum and classical restarts? To characterize the time for search, we utilize the concept of quantum hitting time, or the first-detected-passage time (FDPt). The model we consider is a tight-binding quantum walk with repeated monitoring, which was studied extensively in the absence of restart [49–58]. Such repeated monitoring/measurements have been implemented for example on IBM quantum computers [59]. Our work paves the way to speedup of quantum hitting times, on quantum computers, which as mentioned is particularly important in the presence of dark states.

The benchmark model for classical restart is a diffusive particle whose position is reset at some random time  $t_r$  [9, 10, 19]. In this case the mean time the particle reaches a fixed target is finite (without restart it diverges in an unbounded domain). Further, the mean time to reach a

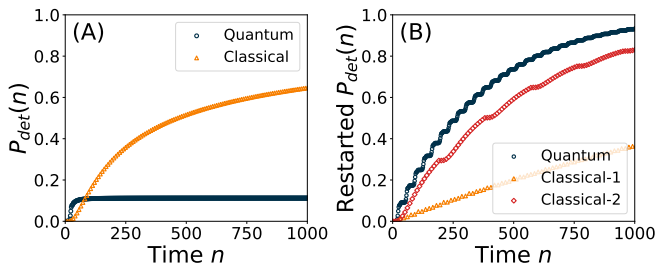


FIG. 2. (A) Detection probability  $P_{\text{det}}(n)$  for a classical/quantum walker on an infinite 1D lattice. The quantum total detection probability  $P_{\text{det}} = \sum_{n=1}^{\infty} F_n \approx 0.1$ , although it grows rapidly at the beginning. The figure illustrated that for short times, the quantum ballistic spreading speeds up the search (compared to the classical counterpart) but at long times the quantum detection without restart performs poorly. (B) Restarted quantum walk performs by far better than the corresponding classical walk, when  $r = 35$  for both models (classical-1). The quantum restart process also performs better if compared with the optimally chosen classical restart (classical-2 when  $r = 191$ ). Here  $\tau = 0.25$ ,  $\delta = 10$ .

target has a distinct minimum, and thus optimal value, as a function of  $t_r$  [9–11, 16, 60]. In contrast, using quantum walks, we will find several minima instead of a unique minimum, and the mean FDPT can exhibit a bi-stable behavior where the hitting time is optimal for a pair of values of  $t_r$ .

Consider a classical random walk on the integers, and let  $P^{\text{cl}}(x, t)$  be the probability of finding the particle on  $x$  at time  $t$ . The master equation is [1]

$$\partial_t P^{\text{cl}}(x, t) = \gamma [P^{\text{cl}}(x+1, t) + P^{\text{cl}}(x-1, t) - 2P^{\text{cl}}(x, t)]. \quad (1)$$

$\gamma$  is the hopping rate. Now consider the tight-binding quantum walk, the wave-function is  $|\psi(t)\rangle = \sum_{-\infty}^{\infty} \phi(x, t)|x\rangle$  and using the Schrödinger equation,

$$-i\partial_t \phi(x, t) = \gamma [\phi(x+1, t) + \phi(x-1, t) - 2\phi(x, t)] \quad (2)$$

with  $\hbar = 1$ . In both models the walker hops to nearest neighbors and the solutions for starting from the origin  $|x\rangle = |0\rangle$  are  $\phi(x, t) = i^x e^{-i2\gamma t} J_x(2\gamma t)$  [54],  $P^{\text{cl}}(x, t) = i^{-x} e^{-2\gamma t} J_x(i2\gamma t)$  [1], where  $J_\alpha(z)$  is the Bessel function of the first kind. Replacing  $t$  with  $it$  one may switch from  $P^{\text{cl}}(x, t)$  to  $\phi(x, t)$ . Still, the packet spreadings are different: the classical packet spreads diffusively and approaches a Gaussian for large times, while the quantum walk propagates ballistically [39].

Quantum systems generally lack precise trajectories. Hence to define first-hitting time we add repeated monitoring at  $|\delta\rangle$ , with the goal to detect the particle at this state. For that an observer makes repeated measurements at times  $\tau, 2\tau, \dots$ . Each measurement is a projection, namely either the particle is found at  $|\delta\rangle$  (yes) or it is not (no), see Fig. 1. This yields a string of measurements, no, no,  $\dots$  and in the  $n$ -th attempt a yes

[50, 52, 54]. The process of search is then completed. Clearly the first time we get a click yes is random, and  $n\tau$  is defined as the hitting time or the FDPT. Note that classically the continuous sampling of the process  $\tau \rightarrow 0$  makes sense, but with the quantum framework this leads to a freeze of the dynamics and to null detection due to the quantum Zeno effect [61].

Let  $F_n$  be the probability of detecting the walker in the  $n$ -th attempt for the first time without restart. Classical and quantum renewal equations were extensively used to obtain these basic probabilities [1, 54]. The quantum  $F_n$ 's are presented in Table I, see also details below and the SM. To start we plot in Fig. 2A the detection probability up to time  $n\tau$ , i.e.  $P_{\text{det}}(n) = \sum_{n'=1}^n F_{n'}$  still without restart (with  $\gamma = 1$ ). We see that at short times  $n\tau$ , the quantum walker is performing better, as it has the advantage of ballistic propagation. However, at large times the classical walker wins in the sense that it is eventually detected with probability one while the quantum system falls far from this limit [55].

To improve the hitting time, we use the sharp-restart strategy [7, 16], leaving other cases to SM, see also further discussion at the end of the letter. Every  $r$  detection attempts we restart the search process, as Fig. 1 depicts. With this approach we find both simple and novel results, we start with the former. Using the simple example in Fig. 2A, if we choose  $r$  to be slightly larger than the time it takes the quantum  $P_{\text{det}}(n)$  to saturate without restart, we observe two effects presented in Fig. 2B. First, the quantum detection is now guaranteed: with probability one we detect the walker in the long time limit (the same for the classical cases). Second, the quantum walker performs much better than the classical one (classical-1), in the sense of a much larger quantum  $P_{\text{det}}(n)$  compared with the classical case. If  $r$  is chosen as the optimal for the classical walk to make a fair comparison, the quantum restart process still performs better than the classical one (classical-2). This is obviously due to the quantum ballistic propagation.

To gain insight, we will focus on the expected FDPT under restart, denoted by  $\langle t_f \rangle_r$ . By definition  $\langle t_f \rangle_r = \tau \langle n_f \rangle_r = \tau (r \langle \mathcal{R} \rangle + \langle \tilde{n} \rangle)$ , where  $n_f$  is the number of measurements until first hitting,  $\mathcal{R}$  is the number of restarts before final detection. Hence  $0 \leq \mathcal{R} \leq \infty$  and  $1 \leq \tilde{n} \leq r$ . The joint distribution of  $\mathcal{R}$  and  $\tilde{n}$  is  $\text{Pr}_r(\mathcal{R}, \tilde{n}) = [1 - P_{\text{det}}(r)]^{\mathcal{R}} F_{\tilde{n}}$ , with the normalization  $\sum_{\mathcal{R}=0}^{\infty} \sum_{\tilde{n}=1}^r \text{Pr}_r(\mathcal{R}, \tilde{n}) = 1$ . Using the restart time  $t_r = r\tau$ , we obtain [7, 30, 62]

$$\langle t_f \rangle_r = \underbrace{\frac{1 - P_{\text{det}}(r)}{P_{\text{det}}(r)} t_r}_{\langle \mathcal{R} \rangle t_r} + \underbrace{\sum_{\tilde{n}=1}^r \frac{(\tilde{n}\tau) F_{\tilde{n}}}{P_{\text{det}}(r)}}_{\tau \langle \tilde{n} \rangle}. \quad (3)$$

(see SM for detailed derivation). In turn, the probabilities  $F_n$  were studied previously in Refs. [54, 55] and as mentioned for small  $n$  are presented in Table I (for  $\delta = 0$ ).

TABLE I.  $F_n$  for the model of an infinite line,  $\delta = 0$ .

| n | $F_n$  |
|---|--|
| 1 | $ J_0(2\gamma\tau) ^2$   |
| 2 | $ J_0(4\gamma\tau) - J_0^2(2\gamma\tau) ^2$  |
| 3 | $ J_0^3(2\gamma\tau) - 2J_0(4\gamma\tau)J_0(2\gamma\tau) + J_0(6\gamma\tau) ^2$  |
| 4 | $  -J_0^4(2\gamma\tau) + 3J_0(4\gamma\tau)J_0^2(2\gamma\tau) - 2J_0(6\gamma\tau)J_0(2\gamma\tau) - J_0^2(4\gamma\tau) + J_0(8\gamma\tau) ^2$ |

The  $F_n$ 's are used to evaluate observables of interest numerically, though clearly as a stand-alone quantity they do not provide much insight. We now focus on the optimization for  $\langle t_f \rangle_r$  in small and large  $\tau$  limits where applicable approximations allow analytical solutions.

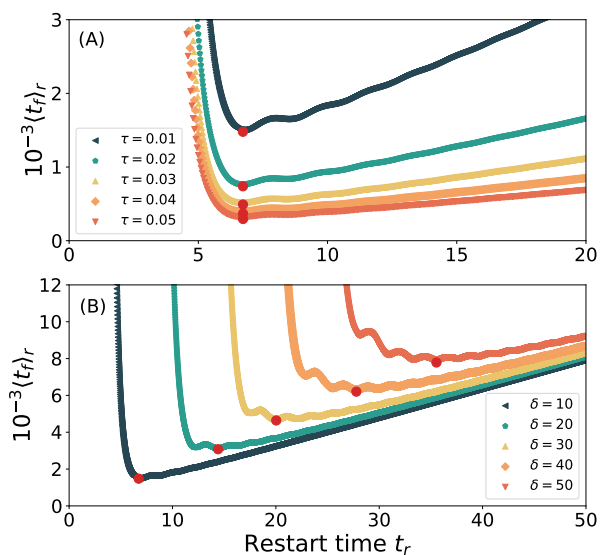


FIG. 3.  $\langle t_f \rangle_r$  vs. restart time  $t_r$  for different  $\delta$  and  $\tau$ , obtained using the repeated-measurement model. The red dots are the minimum calculated using the non-Hermitian approximation Eq. (5). Notice the oscillations which are a quantum feature. We used  $\delta = 10$  (A), and  $\tau = 0.01$  (B). The optimal restart time is  $\tau$  independent (A) while exhibiting a nearly linear dependence on the distance  $\delta$  (B).

*Zeno limit.* We now consider the case where  $\tau$  is small and hence the measurements are frequent. Let  $g(t_f)dt_f$  be the probability of  $t_f$ , in the absence of restart, to be in the interval  $[t_f, t_f + dt_f]$ . In this limit, the process can be modeled with a continuous time formalism, which is a great simplification [52, 57]. This means that we can treat  $g(t_f) = \sum_{n=1} F_n \delta(t_f - n\tau)$  as a smooth function. The main tool here is a non-Hermitian Schrödinger equation,  $i|\dot{\Psi}\rangle = [H - i\hbar(2/\tau)|\delta\rangle\langle\delta|]|\Psi\rangle$ , and  $S(t) = \langle\Psi(t)|\Psi(t)\rangle$  is the probability that the walker “survived” from detection until time  $t$ , and  $g(t_f) = -dS(t)/dt|_{t=t_f}$ . With this approach and  $H$  defined in Eq. (2) one finds

that without restart [56, 63]

$$g(t_f) = \tau \delta^2 \frac{J_\delta^2(2t_f)}{t_f^2}. \quad (4)$$

As  $\tau \rightarrow 0$ , this expression exhibits the well-known Zeno physics, i.e. frequent measurement prohibits state transitions [61]. To remedy this problem we use restart.

Using Eq. (3) in the continuous limit yields

$$\langle t_f \rangle_r \sim \left[ (\delta^2 \tau \mathcal{I}_1)^{-1} - 1 \right] t_r + \mathcal{I}_2 / \mathcal{I}_1, \quad (5)$$

where  $\mathcal{I}_1 = \int_0^{t_r} t_f^{-2} J_\delta^2(2t_f) dt_f$ ,  $\mathcal{I}_2 = \int_0^{t_r} t_f^{-1} J_\delta^2(2t_f) dt_f$  (see SM for explicit solutions). The theory Eq. (5) nicely matches numerical results obtained from the repeated-measurement model (see SM). In Fig. 3, we present  $\langle t_f \rangle_r$  as a function of  $t_r$ , on top of which the global minimum of  $\langle t_f \rangle_r$  (red dots) is provided via minimization of Eq. (5), which remarkably is  $\tau$  ( $\delta$ ) independent (dependent) respectively. We will soon explain this intriguing feature.

We also see in Fig. 3 that for too small or too large  $t_r$ , the mean hitting time diverges as expected. Specifically, using Eq. (5), for  $\delta \neq 0$ ,  $\langle t_f \rangle_r \sim (2\delta - 1)\Gamma^2(1 + \delta)t_r^{2(1-\delta)}/\tau\delta^2$  when  $t_r \rightarrow 0$ , and  $\langle t_f \rangle_r \sim [\pi(4\delta^2 - 1)/8\tau\delta^2 - 1]t_r + (4\delta^2 - 1)\pi/16\delta$  as  $t_r \rightarrow \infty$ . Hence for large  $t_r$  and large  $\delta$ ,  $\langle t_f \rangle_r$  is linear in  $t_r$  with a  $\delta$ -independent slope, which is vastly different from the classical behavior, as the latter is proportional to  $\delta$  [9].

The detection time under restart features oscillations, clearly visible in Fig. 3. These oscillations are in turn related to the phase acquired in  $g(t_f) \sim (\delta^2\tau/\pi)t_f^{-3} \cos^2(2t_f - \pi\delta/2 - \pi/4)$  in large  $t_f$  limit of Eq. (4). The quantum oscillations presented in Fig. 3 imply that we have in general multiple extrema for  $\langle t_f \rangle_r$ , instead of a unique minimum usually found for classical restarts [9–11, 16, 60], see also SM where we present classical examples. Using Eq. (5) the extrema are solutions to

$$\tau\xi - \tau^2 \left[ \xi \int_0^{t_r^{ext}} \tilde{g}(t) dt + \int_0^{t_r^{ext}} t \tilde{g}(t) dt \right] = 0, \quad (6)$$

where  $\tilde{g}(t) = g(t)/\tau$ ,  $\xi = \int_0^{t_r^{ext}} \tilde{g}(t) dt - t_r^{ext} \tilde{g}(t_r^{ext})$ , and the superscript *ext* means extremum. Since  $\tau$  is small we may neglect the  $\tau^2$  terms and find a transcendental equation for the extrema, i.e.  $\xi = 0$  or

$$\int_0^{t_r^{ext}} \frac{J_\delta^2(2t)}{t^2} dt = \frac{J_\delta^2(2t_r^{ext})}{t_r^{ext}}, \quad (7)$$

(see SM for an explicit solution to the integral). Hence the extrema are independent of  $\tau$ , as demonstrated in Fig. 3. Note that similar technique to derive the optimum is used also from classical walks [19, Eq. (7)]. Remarkably, since as mentioned after Eq. (2)  $|J_\delta(2t)|^2$  is the probability of finding the walker at  $|\delta\rangle$ , *in the absence*

of measurements, the extremal restart times are actually connected to the solution of the Schrödinger equation  $|\phi(\delta, t)|^2$ . The transcendental Eq. (7) indicates that the number of extrema increases as  $\delta$  grows. Unlike the classical problem, the global minimum  $t_r^*$  increases roughly linearly with the distance  $\delta$ , and exhibits sudden jumps at special  $\delta$ 's due to the multiple minima (see SM).

*Large  $\tau$  limit.* Also when the measurement period  $\tau$  is large we find interesting effects. In this case and without restart the probability of FDPt  $F_n$  is given by the wavefunction of the system in the absence of measurements. The origin of this effect is that sparse measurements do not modify the Hermitian dynamics too much. Specifically, using the asymptotics of the Bessel function [54, 65]

$$F_n(\tau) = |\langle 0|\psi(t = n\tau)|\rangle|^2 \sim \frac{1}{n\pi\tau} \cos^2\left(2n\tau - \frac{\pi}{4}\right). \quad (8)$$

Here we have focused on the case called the return problem when  $\delta = 0$ , partly due to space limitation. In Fig. 4 we plot  $r^* = t_r^*/\tau$  versus  $\tau$  using a numerically exact calculation. Clearly unlike the Zeno case, now  $\tau$  is an important parameter. Remarkably as shown in Fig. 4,  $r^*$  exhibits a periodic sequence of staircases, which are now analyzed.

Beyond the fact we get for the optimum  $r^*$  periodic-like behavior, there are plunges for certain critical  $\tau$ 's in Fig. 4. This means that the optimal restart step jumps from  $r^* = 6$  to  $r^* = 1$ , when  $\tau$  is only slightly modified. This indicates the existence of instabilities in the system, related to quantum oscillations. To understand these effects, we used Eq. (8). First notice that choosing  $2\tau$  as a multiple of  $\pi$ , we have  $F_n \sim 1/(2n\pi\tau)$ . Since  $F_n$  is monotonically decaying with  $n$ , it is not difficult to realize that the optimal strategy to restart is to choose  $r^* = 1$ , namely immediate restart (this holds in the classical counterpart since the first-passage probability decays as  $t^{-3/2}$  [1]). This explains the periodicity presented in Fig. 4. As we vary  $\tau$ , then close to  $\tau = k\pi/2$  with  $k$  a positive integer, the best strategy is to restart as fast as possible, i.e.  $r^* = 1$ .

What will happen when we increase  $\tau$ ? Considering the mean  $\langle n_f \rangle_r = \langle t_f \rangle_r / \tau$ , note that  $\langle n_f \rangle_1 = 1/F_1$  and importantly when  $\tau$  is large, such that  $F_n \ll 1$  we have  $\langle n_f \rangle_2 \sim 2/(F_1 + F_2)$ ,  $\langle n_f \rangle_3 \sim 3/(F_1 + F_2 + F_3)$  etc. Let  $\tau = k\pi/2 + \epsilon$  and  $0 < \epsilon < \pi/2$ . As mentioned for  $\epsilon = 0$ ,  $r^* = 1$ . When the condition  $\langle n_f \rangle_1 = \langle n_f \rangle_2$  holds, there is a transition from  $r^* = 1$  to  $r^* = 2$  taking place when  $\epsilon_{1 \rightarrow 2} = 0.850$  (see derivation in SM). Further transitions in  $r^*$  from  $r$  to  $r + 1$  take place whenever

$$rF_{r+1} = \sum_{n=1}^r F_n. \quad (9)$$

Importantly this formula admits a finite number of solutions, which based on physical intuition is expected, since  $r^*$  cannot be too large. Using Eqs. (8,9) we find those

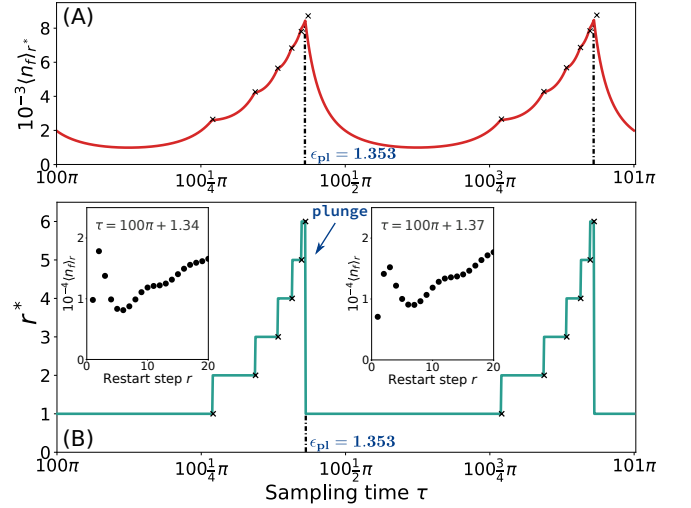


FIG. 4. (A)  $\langle n_f \rangle_{r^*}$  versus  $\tau$ .  $\langle n_f \rangle_{r^*} \sim 1/F_{r^*+1}$  is used to calculate the theoretical optima at transition points (black crosses), around which nonsmoothness is witnessed. (B) The optimal restart step  $r^*$  versus  $\tau$ . We see the novel staircase structure in large  $\tau$ , however this type of behavior appears in the full range of  $\tau$  (see SM). The black crosses represent the theoretical transition  $\tau$ 's Eq. (10). For classical restart,  $r^* = 1$ . The insets present  $\langle n_f \rangle_r$  vs.  $r$  in the vicinity of the plunge  $\tau (= 100\pi + 1.353)$ . There are two minima competing with each other, and a small change of  $\tau$  (i.e.  $\Delta\tau = 0.03$ ) results in different optima. On the left inset  $r^* = 6$  and on the right  $r^* = 1$ . We used  $\delta = 0$ .

$\epsilon_{j \rightarrow j+1}$  on which the step-like jumps take place, with  $j$  increasing from 1 till 5,

$$\{\epsilon_{j \rightarrow j+1}\} = \{0.850, 1.081, 1.204, 1.280, 1.332\}, \epsilon_{pl} = 1.353. \quad (10)$$

The subscript *pl* means plunge, i.e. the jump from  $r^* = 6$  to  $r^* = 1$ . Thus as shown in Fig. 4 we have a complete theory of the staircase structure. Further using the smallness of  $F_n$  we have at transition points  $\langle n_f \rangle_{r^*} \sim 1/F_{r^*+1}$ .

To better understand the ‘‘plunge’’ namely the transition  $r^* = 6 \rightarrow r^* = 1$  found for  $\epsilon_{pl}$ ,  $\langle n_f \rangle_r$  close to a critical value of  $\tau$  is plotted in the insets of Fig. 4. There appear two minima of  $\langle n_f \rangle_r$ . The first is at  $r^* = 6$  and the second at  $r^* = 1$ . A slight change of  $\tau$  leads to the global minimum switching from one value to the other. At the exact transition value, the two minima are identical. Thus the system exhibits an instability in the sense that small changes of  $\tau$  create a large difference in  $r^*$ .

*Discussion.* Employing the sharp-restart strategy, we expedite the hitting time of a tight-binding quantum walk and now we emphasize three points. First, the expected hitting time under restart exhibits an oscillatory behavior unlike the classical case, rendering the appearance of several extrema. This effect is general and not limited to the Zeno limit, as we will show in a future publication. What is unique to this limit, is that the optimal restart is  $\tau$ -independent, and that one may obtain



a transcendental equation which is a by far simpler tool if compared with an exact though numerical evaluation of the problem. Second, previously it was shown that sharp restart has certain advantage of attaining the lowest mean passage time among all restart strategies [7, 16]. It is also noteworthy that the quantum feature of oscillations is wiped out with Poisson or geometric restarts (see details in SM), thus sharp restart should be used in the quantum domain. Third, in sparse measurement limit, i.e. large  $\tau$ , the optimal restart step  $r^*$  exhibits a periodical staircase structure with instabilities, i.e. plunges in the optimal restart time (Fig. 4). We expect these instabilities to be generic for a wide range of parameter changes, as their cause is the oscillatory nature of the detection time statistics. These plunges and instabilities are clearly a signature of the quantum dynamics, and as far as we know, are new in the general framework of restart theory.

Our theory can be implemented in laboratories, as restarts are routinely used, for the aim of repeating experimental protocols to gain statistics of various outputs. Probably the best way to test the theory is on quantum computers. Here the repeated strong measurements needed for hitting time statistics and the restarts i.e. the returning of the system to its initial state, are now built in parts of quantum computing package. The quantum walk part is implemented by the Jordan-Wigner transformation, that maps the walk to a qubit representation [59]. It should be noted that system size does not have to be large, as some of the effects we found here, like staircases and plunges (Fig. 4) are generic to all quantum systems.

The support of Israel Science Foundation's grant 1614/21 is acknowledged.

---

[1] S. Redner, *A Guide to First-Passage Processes* (Cambridge University Press, 2001).

[2] R. Metzler, G. Oshanin, and S. Redner, *First-Passage Phenomena and Their Applications* (World Scientific, 2014).

[3] B. Munsky, I. Nemenman, and G. Bel, *Journal of Chemical Physics* **131**, 235103 (2009).

[4] G. Bel, B. Munsky, and I. Nemenman, *Physical Biology* **7**, 016003 (2009).

[5] S. Reuveni, M. Urbakh, and J. Klafter, *Proceedings of the National Academy of Sciences of the United States of America* **111** (2014), 10.1073/pnas.1318122111.

[6] T. Rotbart, S. Reuveni, and M. Urbakh, *Phys. Rev. E* **92**, 060101 (2015).

[7] M. Luby, A. Sinclair, and D. Zuckerman, [1993] The 2nd Israel Symposium on Theory and Computing Systems, 128 (1993).

[8] C. P. Gomes, B. Selman, and H. A. Kautz, in *AAAI/IAAI* (1998).

[9] M. R. Evans and S. N. Majumdar, *Phys. Rev. Lett.* **106**, 160601 (2011).

[10] M. R. Evans and S. N. Majumdar, *Journal of Physics A: Mathematical and Theoretical* **44**, 435001 (2011).

[11] M. R. Evans and S. N. Majumdar, *Journal of Physics A: Mathematical and Theoretical* **47**, 285001 (2014).

[12] D. Boyer and C. Solis-Salas, *Phys. Rev. Lett.* **112**, 240601 (2014).

[13] S. Gupta, S. N. Majumdar, and G. Schehr, *Phys. Rev. Lett.* **112**, 220601 (2014).

[14] S. Eule and J. J. Metzger, *New Journal of Physics* **18**, 033006 (2016).

[15] S. Reuveni, *Phys. Rev. Lett.* **116**, 170601 (2016).

[16] A. Pal and S. Reuveni, *Phys. Rev. Lett.* **118**, 030603 (2017).

[17] A. Falc3n-Cort3s, D. Boyer, L. Giuggioli, and S. N. Majumdar, *Phys. Rev. Lett.* **119**, 140603 (2017).

[18] S. Belan, *Phys. Rev. Lett.* **120**, 080601 (2018).

[19] A. Chechkin and I. M. Sokolov, *Phys. Rev. Lett.* **121**, 050601 (2018).

[20] M. R. Evans and S. N. Majumdar, *Journal of Physics A: Mathematical and Theoretical* **51**, 475003 (2018).

[21] D. Boyer, A. Falc3n-Cort3s, L. Giuggioli, and S. N. Majumdar, *Journal of Statistical Mechanics: Theory and Experiment* **2019**, 053204 (2019).

[22] A. S. Bodrova, A. V. Chechkin, and I. M. Sokolov, *Phys. Rev. E* **100**, 012120 (2019).

[23] A. S. Bodrova, A. V. Chechkin, and I. M. Sokolov, *Phys. Rev. E* **100**, 012119 (2019).

[24] L. Ku3mierz and E. Gudowska-Nowak, *Phys. Rev. E* **99**, 052116 (2019).

[25] B. Besga, A. Bovon, A. Petrosyan, S. N. Majumdar, and S. Ciliberto, *Phys. Rev. Research* **2**, 032029 (2020).

[26] M. Magoni, S. N. Majumdar, and G. Schehr, *Phys. Rev. Research* **2**, 033182 (2020).

[27] M. R. Evans, S. N. Majumdar, and G. Schehr, *Journal of Physics A: Mathematical and Theoretical* **53**, 193001 (2020).

[28] B. De Bruyne, J. Randon-Furling, and S. Redner, *Phys. Rev. Lett.* **125**, 050602 (2020).

[29] O. Tal-Friedman, A. Pal, A. Sekhon, S. Reuveni, and Y. Roichman, *The Journal of Physical Chemistry Letters* **11**, 7350 (2020).

[30] I. Eliazar and S. Reuveni, *Journal of Physics A: Mathematical and Theoretical* **54**, 125001 (2021).

[31] B. D. Bruyne, J. Randon-Furling, and S. Redner, *Journal of Statistical Mechanics: Theory and Experiment* **2021**, 013203 (2021).

[32] V. M3endez, A. Mas3-Puigdellosas, T. Sandev, and D. Campos, *Phys. Rev. E* **103**, 022103 (2021).

[33] S. N. Majumdar, F. Mori, H. Schawe, and G. Schehr, *Phys. Rev. E* **103**, 022135 (2021).

[34] M. Dahlenburg, A. V. Chechkin, R. Schumer, and R. Metzler, *Phys. Rev. E* **103**, 052123 (2021).

[35] R. K. Singh, T. Sandev, A. Iomin, and R. Metzler, (2021), arXiv:2105.08112.

[36] Y. Aharonov, L. Davidovich, and N. Zagury, *Phys. Rev. A* **48**, 1687 (1993).

[37] E. Farhi and S. Gutmann, *Phys. Rev. A* **58**, 915 (1998).

[38] J. Kempe, *Contemporary Physics* **44**, 307 (2003), <https://doi.org/10.1080/00107151031000110776>.

[39] Y. Lahini, A. Avidan, F. Pozzi, M. Sorel, R. Morandotti, D. N. Christodoulides, and Y. Silberberg, *Phys. Rev. Lett.* **100**, 013906 (2008).

[40] O. M3ulken and A. Blumen, *Physics Reports* **502**, 37 (2011).

- [41] B. Mukherjee, K. Sengupta, and S. N. Majumdar, *Phys. Rev. B* **98**, 104309 (2018).
- [42] D. C. Rose, H. Touchette, I. Lesanovsky, and J. P. Garrahan, *Phys. Rev. E* **98**, 022129 (2018).
- [43] S. Belan and V. Parfenyev, *New Journal of Physics* **22**, 073065 (2020).
- [44] G. Peretto, F. Carollo, M. Magoni, and I. Lesanovsky, *Phys. Rev. B* **104**, L180302 (2021).
- [45] G. Peretto, F. Carollo, and I. Lesanovsky, (2021), [arXiv:2112.05078](https://arxiv.org/abs/2112.05078).
- [46] X. Turkeshi, M. Dalmonte, R. Fazio, and M. Schirò, (2021), [arXiv:2111.03500](https://arxiv.org/abs/2111.03500).
- [47] M. Magoni, F. Carollo, G. Peretto, and I. Lesanovsky, (2022), [arXiv:2202.12655](https://arxiv.org/abs/2202.12655).
- [48] F. Caruso, A. W. Chin, A. Datta, S. F. Huelga, and M. B. Plenio, *The Journal of Chemical Physics* **131**, 105106 (2009).
- [49] F. Thiel, I. Mualem, D. Meidan, E. Barkai, and D. A. Kessler, *Phys. Rev. Research* **2**, 043107 (2020).
- [50] H. Krovi and T. A. Brun, *Phys. Rev. A* **74**, 042334 (2006).
- [51] F. A. Grünbaum, L. Velázquez, A. H. Werner, and R. F. Werner, *Communications in Mathematical Physics* **320**, 543 (2013).
- [52] S. Dhar, S. Dasgupta, A. Dhar, and D. Sen, *Phys. Rev. A* **91**, 062115 (2015).
- [53] S. Dhar, S. Dasgupta, and A. Dhar, *Journal of Physics A: Mathematical and Theoretical* **48**, 115304 (2015).
- [54] H. Friedman, D. A. Kessler, and E. Barkai, *Phys. Rev. E* **95**, 032141 (2017).
- [55] F. Thiel, E. Barkai, and D. A. Kessler, *Phys. Rev. Lett.* **120**, 040502 (2018).
- [56] F. Thiel and D. A. Kessler, *Phys. Rev. A* **102**, 012218 (2020).
- [57] V. Dubey, C. Bernardin, and A. Dhar, *Phys. Rev. A* **103**, 032221 (2021).
- [58] D. Das and S. Gupta, *Journal of Statistical Mechanics: Theory and Experiment* **2022**, 033212 (2022).
- [59] S. Tornow and K. Ziegler, (2022), [arXiv:2210.09941](https://arxiv.org/abs/2210.09941).
- [60] S. Gupta and A. M. Jayannavar, *Frontiers in Physics* **10** (2022), 10.3389/fphy.2022.789097.
- [61] B. Misra and E. C. G. Sudarshan, *Journal of Mathematical Physics* **18**, 756 (1977).
- [62] O. L. Bonomo and A. Pal, *Phys. Rev. E* **103**, 052129 (2021).
- [63] P. L. Krapivsky, J. M. Luck, and K. Mallick, *Journal of Statistical Physics* **154**, 1430 (2014).
- [64] O. L. Bonomo and A. Pal, (2021), [arXiv:2106.14036](https://arxiv.org/abs/2106.14036).
- [65] Eq. (8) is valid for not too large  $n$ , however, since our main results focus on finite  $r$  restart, the approximation Eq. (8) holds.

### General stochastic restart strategies

In the Letter we studied the quantum first detection problem with a sharp restart strategy. We now develop the theory for more general restart processes, namely the case when the restart times are randomly distributed. More precisely, the time intervals between restarts are independent and identically distributed discrete random variables, denoted with  $r$ . At the end of the section we

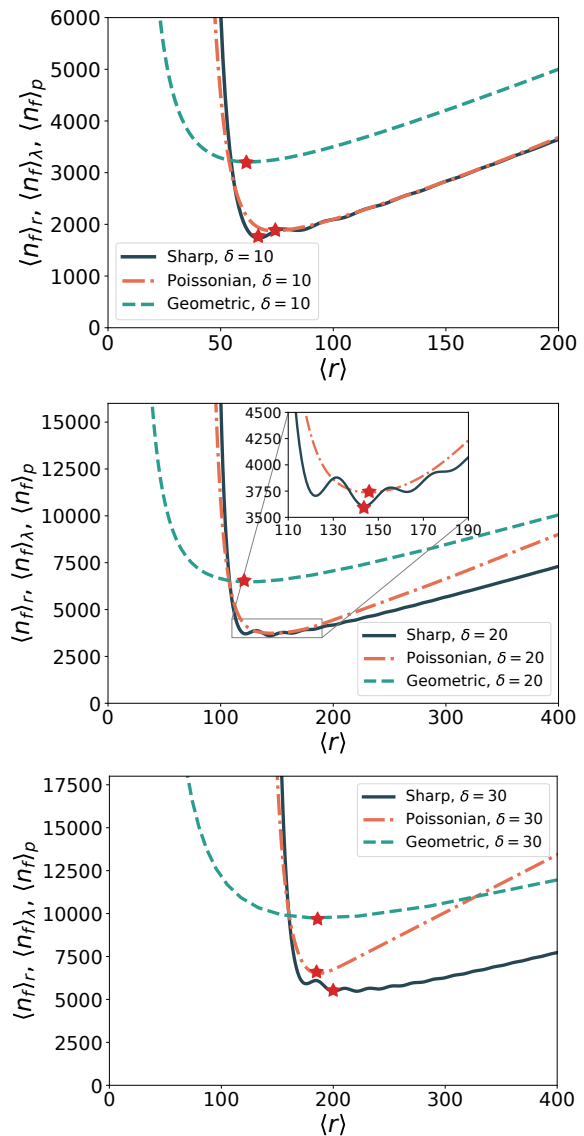


FIG. 5. A comparison between sharp, Poisson, geometric distributed restart strategies, the mean  $\langle n_f \rangle_R$  vs. the mean restart step  $\langle r \rangle$ . The sampling time is set as  $\tau = 0.1$ . As expected, the quantum oscillations are captured only by the sharp restart, see the inset for zoom-in, and Eqs. (16,20,22). As mentioned in the main text, the mean hitting time with sharp restart takes the lowest minimum, see the red stars denoting each minimum. For  $\delta = 10$ ,  $\min(\langle n_f \rangle_r) = 1734$ ,  $\min(\langle n_f \rangle_\lambda) = 1874$ ,  $\min(\langle n_f \rangle_p) = 3209$ . For  $\delta = 20$ ,  $\min(\langle n_f \rangle_r) = 3607$ ,  $\min(\langle n_f \rangle_\lambda) = 3736$ ,  $\min(\langle n_f \rangle_p) = 6488$ . For  $\delta = 30$ ,  $\min(\langle n_f \rangle_r) = 5473$ ,  $\min(\langle n_f \rangle_\lambda) = 6515$ ,  $\min(\langle n_f \rangle_p) = 9743$ . See also the inset for confirmation.

will present the mean first detection time under restart, for sharp restart, Poisson restart and geometric restart, see Fig. 5 below. The goal is to study the quantum oscillations in Fig. 3 in the main text, and to see whether they are found also for other distributions of waiting times. For that we need a new formalism. We start from the general framework proposed recently in Refs. [16, 62],

which states that the mean hitting time with a restart strategy  $R$  (performing restarts at random time  $r$ ) is

$$\langle n_f \rangle_R = \frac{\langle \min(n, r) \rangle}{P(n \leq r)}, \quad (11)$$

where  $n$  is the first hitting time in the absence of restart, and the numerator means the expectation of the minimum of  $n$  and the random restart time/step  $r$ . And hereinafter we denote  $P(\text{cond})$  as the probability that the condition  $\text{cond}$  is satisfied. We note that

$$\begin{aligned} \langle \min(n, r) \rangle &= \sum_{k=1}^{\infty} k P(r = k) \left( 1 - \sum_{n=1}^{k-1} F_n \right) \\ &\quad + \sum_{n=1}^{\infty} n F_n \sum_{k=n+1}^{\infty} P(r = k), \quad (12) \\ P(n \leq r) &= \sum_{n=1}^{\infty} F_n \sum_{k=n}^{\infty} P(r = k). \end{aligned}$$

Here we used the normalization of  $P(r = k)$ , the later is the probability that the time interval between restarts is  $k$ . In what follows in the section, we will provide formulae for the mean hitting time with Poisson, geometric and sharp restart, which were already studied in [64] where the classical first passage time is considered.

**Poisson restart.** Assuming the restart obeys the Poisson distribution, namely,

$$P(r = k) = \frac{e^{-\lambda} \lambda^{k-1}}{(k-1)!}, \quad k \geq 1. \quad (13)$$

The value of  $k$  is shifted so that  $P(r = k)$  for  $k \geq 1$  is normalized. The mean of restart step is determined by the parameter  $\lambda$ , indicated by  $\langle r \rangle = \sum_{k=1}^{\infty} k P(r = k) = 1 + \lambda$ . Eq. (13) allows the simplification of the following:

$$\begin{aligned} \langle \min(n, r) \rangle &= \sum_{k=1}^{\infty} k \frac{e^{-\lambda} \lambda^{k-1}}{(k-1)!} - \sum_{k=1}^{\infty} k \frac{e^{-\lambda} \lambda^{k-1}}{(k-1)!} \sum_{n=1}^{k-1} F_n \\ &\quad + \sum_{n=1}^{\infty} n F_n \sum_{k=n+1}^{\infty} \frac{e^{-\lambda} \lambda^{k-1}}{(k-1)!} \\ &= 1 + \lambda - \sum_{n=1}^{\infty} F_n \sum_{k=n+1}^{\infty} k \frac{e^{-\lambda} \lambda^{k-1}}{(k-1)!} \\ &\quad + \sum_{n=1}^{\infty} n F_n \sum_{k=n+1}^{\infty} \frac{e^{-\lambda} \lambda^{k-1}}{(k-1)!} \quad (14) \\ &= 1 + \lambda - \sum_{n=1}^{\infty} F_n \sum_{k=n+1}^{\infty} (k-n) \frac{e^{-\lambda} \lambda^{k-1}}{(k-1)!}, \\ P(n \leq r) &= \sum_{n=1}^{\infty} F_n \sum_{k=n}^{\infty} \frac{e^{-\lambda} \lambda^{k-1}}{(k-1)!}. \end{aligned}$$

We note

$$\begin{aligned} \sum_{k=n}^{\infty} \frac{e^{-\lambda} \lambda^{k-1}}{(k-1)!} &= 1 - \frac{\Gamma(n-1, \lambda)}{\Gamma(n-1)} =: \alpha(n, \lambda), \\ \sum_{k=n+1}^{\infty} k \frac{e^{-\lambda} \lambda^{k-1}}{(k-1)!} &= \frac{e^{-\lambda} \lambda^{n+1} - \lambda \Gamma(n+1, \lambda)}{\Gamma(n+1)} \\ &\quad + \frac{e^{-\lambda} \lambda^n - \Gamma(n, \lambda)}{\Gamma(n)} + 1 + \lambda \\ &=: \beta(n+1, \lambda). \end{aligned} \quad (15)$$

where  $\Gamma(a, z)$  is the upper incomplete gamma function, and  $\Gamma(z)$  is the gamma function. Thus the mean hitting time with Poisson restart is

$$\langle n_f \rangle_{\lambda} = \frac{1 + \lambda - \sum_{n=1}^{\infty} F_n [\beta(n+1, \lambda) - n \alpha(n+1, \lambda)]}{\sum_{n=1}^{\infty} F_n \alpha(n, \lambda)}. \quad (16)$$

We note that in the extreme case of  $\lambda = 0$ ,  $P(r = k) = \frac{e^{-\lambda} \lambda^{k-1}}{(k-1)!} = \delta_{k,1}$ , namely a deterministic/sharp restart at  $r = 1$ , and straightforward calculation also yields  $\langle n_f \rangle_{\lambda=0} = 1/F_1$ , which is exactly the mean under sharp restart at  $r = 1$ .

**Geometric restart.** Considering the restart step  $r$  obeying the geometric distribution, which is a discrete version of the exponential distribution, namely,

$$P(r = k) = (1-p)^{k-1} p, \quad k \geq 1. \quad (17)$$

We shift the conventional form by unity since the restart happens from  $r = 1$ . The parameter  $p$  dominates the mean of restart step, i.e.  $\langle r \rangle = 1/p$ . With Eq. (17), and Eqs. (11,12), we have [62]

$$\begin{aligned} \langle \min(n, r) \rangle &= \sum_{k=1}^{\infty} k p (1-p)^{k-1} - \sum_{k=1}^{\infty} k p (1-p)^{k-1} \sum_{n=1}^{k-1} F_n \\ &\quad + \sum_{n=1}^{\infty} n F_n \sum_{k=n+1}^{\infty} p (1-p)^{k-1} \\ &= \frac{1}{p} - \sum_{n=1}^{\infty} F_n \sum_{k=n+1}^{\infty} k p (1-p)^{k-1} + \sum_{n=1}^{\infty} n F_n \sum_{k=n+1}^{\infty} p (1-p)^{k-1} \\ &= \frac{1}{p} - \frac{1}{p} \sum_{n=1}^{\infty} F_n (1-p)^n (1+np) + \sum_{n=1}^{\infty} n F_n (1-p)^n \\ &= \frac{1}{p} \left[ 1 - \sum_{n=1}^{\infty} F_n (1-p)^n \right] \quad (18) \end{aligned}$$

and

$$\begin{aligned} P(n \leq r) &= \sum_{n=1}^{\infty} F_n \sum_{k=n}^{\infty} (1-p)^{k-1} p \\ &= \sum_{n=1}^{\infty} F_n (1-p)^{n-1} = (1-p)^{-1} \sum_{n=1}^{\infty} F_n (1-p)^n. \end{aligned} \quad (19)$$

Hence the mean hitting time with geometric restart, denoted by  $\langle n_f \rangle_p$ , is expressed as

$$\langle n_f \rangle_p = \frac{1-p}{p} \frac{1 - \sum_{n=1}^{\infty} F_n (1-p)^n}{\sum_{n=1}^{\infty} F_n (1-p)^n}. \quad (20)$$

**Sharp restart.** The sharp-restart strategy is deterministic, and the probability mass function of  $r$  is

$$P(r=k) = \delta_{k,r'}, \quad k \geq 1, \quad (21)$$

which gives the mean  $\langle r \rangle = r'$  directly. For simplicity, we will use  $r$  as the mean, to replace  $r'$ . Then Eq. (11) gives

$$\langle n_f \rangle_r = r \frac{1 - P_{\text{det}}(r)}{P_{\text{det}}(r)} + \frac{\sum_{n=1}^r n F_n}{P_{\text{det}}(r)}. \quad (22)$$

Multiplying both sides of Eq. (22) by the measurement period  $\tau$  gives the Eq. (3) in the main text. Alternatively, we provide here another straightforward derivation for the mean in this case, using the first hitting probability under sharp restart. With some fixed restart step at  $r$ , the first hitting at  $n = r\mathcal{R} + \tilde{n}$  ( $\mathcal{R} \geq 0$  is the number of restarts happened,  $1 \leq \tilde{n} \leq r$ ) occurs with probability

$$F_n^{(r)} = \left[1 - P_{\text{det}}(r)\right]^{\mathcal{R}} F_{\tilde{n}}, \quad (23)$$

where the superscript  $(r)$  means the deterministic restart time at step  $r$ . By definition,  $\mathcal{R} = \lfloor (n-1)/r \rfloor$  with  $\lfloor \cdot \rfloor$  means the integer part, and  $\tilde{n} = n - r\mathcal{R} = 1 + \text{mod}(n-1, r)$ . Then the mean hitting time with sharp restart is

$$\begin{aligned} \langle n_f \rangle_r &= \sum_{n=1}^{\infty} n F_n^{(r)} = \sum_{r\mathcal{R} + \tilde{n} = 1}^{\infty} n \left[1 - P_{\text{det}}(r)\right]^{\mathcal{R}} F_{\tilde{n}} \\ &= \sum_{\mathcal{R}=0}^{\infty} \sum_{\tilde{n}=1}^r (r\mathcal{R} + \tilde{n}) \left[1 - P_{\text{det}}(r)\right]^{\mathcal{R}} P_{\text{det}}(r) F_{\tilde{n}}/P_{\text{det}}(r) \\ &= r \underbrace{\sum_{\mathcal{R}=0}^{\infty} \mathcal{R} P_{\text{det}}(r) \left[1 - P_{\text{det}}(r)\right]^{\mathcal{R}}}_{\langle \mathcal{R} \rangle} \underbrace{\sum_{\tilde{n}=1}^r F_{\tilde{n}}/P_{\text{det}}(r)}_{=1} \\ &\quad + \underbrace{\sum_{\tilde{n}=1}^r \tilde{n} F_{\tilde{n}}/P_{\text{det}}(r)}_{\langle \tilde{n} \rangle} \underbrace{\sum_{\mathcal{R}=0}^{\infty} P_{\text{det}}(r) \left[1 - P_{\text{det}}(r)\right]^{\mathcal{R}}}_{=1} \\ &= \underbrace{\frac{r[1 - P_{\text{det}}(r)]}{P_{\text{det}}(r)}}_{r\langle \mathcal{R} \rangle} + \underbrace{\sum_{\tilde{n}=1}^r \frac{\tilde{n} F_{\tilde{n}}}{P_{\text{det}}(r)}}_{\langle \tilde{n} \rangle}. \end{aligned} \quad (24)$$

This agrees with Eq. (22). The formula depicts a clear probabilistic picture: the expectation of first hitting at  $n = r\mathcal{R} + \tilde{n}$  is equal to the expected number of restarts happened,  $\langle \mathcal{R} \rangle$ , with  $\mathcal{R}$  obeying the geometric distribution  $G(\mathcal{R} = k) = P_{\text{det}}(r)[1 - P_{\text{det}}(r)]^k$  with

$k = 0, 1, 2, \dots$ , multiplied by  $r$ , plus the expected number of attempts till hitting following the last restart, conditioned successful click before the next restart, namely  $\langle \tilde{n} \rangle$ , with  $\tilde{n}$  distributed by  $F_{\tilde{n}}/P_{\text{det}}(r)$ .

We are now ready to study the effect of random time intervals between restarts. In Fig. 5 of this supplemental material we plot the mean of the restarted hitting time  $\langle n_f \rangle_R$  versus the mean of restart time  $r$  for the three distributions studied here. We do so for different initial states, namely the distance between the detected state and the initial state denoted  $\delta$ , on the one dimensional lattice is varied. Then we manipulate  $\langle r \rangle$  (the  $x$  axis of the plot), e.g. for Poisson case we vary the parameter  $\lambda$ , etc. Using  $F_n$ 's obtained from the quantum renewal equation, see Sec. below, we can plot these curves without effort. The main observation are that: a) Poisson and geometric distributions do not give any visible oscillations and b) that the global minimum of the restarted process is always found for the sharp restart. The observation a) is related to the wipe out of coherence due to the randomness of the time interval between restarts. The second effect, as mentioned, is due to the general theorem studied in [7], and in the next section. It is left for future studies to study if other distributions of times between restarts can yield oscillations beyond the sharp case, for example very narrow distributions around the mean, which are not totally sharp, are expected to give some oscillations as well.

### Proof for the dominance of sharp-restart strategy

Here we prove that the sharp-restart strategy outperforms any other restart strategy, in the sense of always attaining the smallest minimum of the expected  $n_f$  [7, 16]. We follow the work of mathematicians [7] and see alternative proof in Ref. [16].

Assuming a sequence of waiting times between restarts,  $\vec{S} = \{r_1, r_2, r_3, \dots\}$ , with  $r_i$  being positive integers, the restarts are performed at steps  $n = r_1, r_1 + r_2, r_1 + r_2 + r_3, \dots$ , and the process is stopped in the first hitting. Then the possible values of  $n_f$  will be  $n_f = \sum_{i=1}^j r_i + \tilde{n}$ , where  $j$  is the number of restarts happened, taking natural numbers, and  $\tilde{n}$  is the time between the first hitting and the final restart,  $1 \leq \tilde{n} \leq r_{j+1}$ . Hence the probability of  $n_f$  (with the time sequence  $\vec{S}$ ) is  $F_n^{\vec{S}} = \prod_{i=1}^j [1 - P_{\text{det}}(r_i)] F_{\tilde{n}}$ , where  $P_{\text{det}}(r_i) = \sum_{n=1}^{r_i} F_n$ , and



the mean of  $n_f$  is

$$\begin{aligned}
\langle n_f \rangle_{\vec{S}} &= \sum_{i=1}^{\infty} \sum_{\tilde{n}=1}^{r_i} \left( \sum_{j=1}^{i-1} r_j + \tilde{n} \right) \prod_{k=1}^{i-1} [1 - P_{\text{det}}(r_k)] F_{\tilde{n}} \\
&= \sum_{i=1}^{\infty} (r_1 + r_2 + \dots + r_{i-1}) \prod_{j=1}^{i-1} [1 - P_{\text{det}}(r_j)] P_{\text{det}}(r_i) \\
&\quad + \sum_{i=1}^{\infty} \left\{ \prod_{j=1}^{i-1} [1 - P_{\text{det}}(r_j)] \right\} \sum_{\tilde{n}=1}^{r_i} \tilde{n} F_{\tilde{n}} \\
&= \sum_{i=1}^{\infty} r_i \sum_{j=i}^{\infty} \prod_{k=1}^j [1 - P_{\text{det}}(r_k)] P_{\text{det}}(r_{j+1}) \\
&\quad + \sum_{i=1}^{\infty} \left\{ \prod_{j=1}^{i-1} [1 - P_{\text{det}}(r_j)] \right\} \sum_{\tilde{n}=1}^{r_i} \tilde{n} F_{\tilde{n}}.
\end{aligned} \tag{25}$$

Note that

$$\begin{aligned}
&\sum_{j=i}^{\infty} \prod_{k=1}^j [1 - P_{\text{det}}(r_k)] P_{\text{det}}(r_{j+1}) \\
&= \sum_{j=i}^{\infty} P \left( \sum_{k=1}^j r_k < n_f \leq \sum_{k=1}^{j+1} r_k \right) \\
&= P \left( n_f > \sum_{k=1}^i r_k \right).
\end{aligned} \tag{26}$$

We now related between  $\langle n_f \rangle_{\vec{S}}$  for a general sequence and  $\langle n_f \rangle_r$  for sharp restart. Recall that for sharp restart and hence for  $\langle n_f \rangle_r$  the waiting times between restarts just become  $\{r, r, r, \dots\}$ . We use Eq. (22) to solve for  $\sum_{\tilde{n}=1}^{r_i} \tilde{n} F_{\tilde{n}}$ , namely for sharp restart,

$$\begin{aligned}
\langle n_f \rangle_r &= r \frac{1 - P_{\text{det}}(r)}{P_{\text{det}}(r)} + \sum_{\tilde{n}=1}^r \frac{\tilde{n} F_{\tilde{n}}}{P_{\text{det}}(r)} \\
\Rightarrow \sum_{\tilde{n}=1}^{r_i} \tilde{n} F_{\tilde{n}} &= P_{\text{det}}(r_i) \langle n_f \rangle_{r_i} - r_i [1 - P_{\text{det}}(r_i)],
\end{aligned} \tag{27}$$

where  $\langle n_f \rangle_{r_i}$  is the mean of  $n_f$  with sharp restart at  $r_i$ , or with the waiting time (between restarts) sequence  $\{r_i, r_i, r_i, \dots\}$ . With Eqs. (26,27), Eq. (25) becomes

$$\begin{aligned}
\langle n_f \rangle_{\vec{S}} &= \sum_{i=1}^{\infty} r_i P \left( n_f > \sum_{k=1}^i r_k \right) + \sum_{i=1}^{\infty} \left\{ \prod_{j=1}^{i-1} [1 - P_{\text{det}}(r_j)] \right\} \\
&\quad \times \left\{ P_{\text{det}}(r_i) \langle n_f \rangle_{r_i} - r_i [1 - P_{\text{det}}(r_i)] \right\} \\
&= \sum_{i=1}^{\infty} \left\{ \prod_{j=1}^{i-1} [1 - P_{\text{det}}(r_j)] \right\} P_{\text{det}}(r_i) \langle n_f \rangle_{r_i} \\
&= \sum_{i=1}^{\infty} P \left( \sum_{k=1}^{i-1} r_k < n_f \leq \sum_{k=1}^i r_k \right) \langle n_f \rangle_{r_i},
\end{aligned} \tag{28}$$

where we employed the relation

$$P \left( n_f > \sum_{k=1}^i r_k \right) = \prod_{j=1}^{i-1} [1 - P_{\text{det}}(r_j)] [1 - P_{\text{det}}(r_i)]. \tag{29}$$

We now use the technique presented in [7]. Since  $P \left( \sum_{k=1}^{i-1} r_k < n_f \leq \sum_{k=1}^i r_k \right)$  is normalized, we obtain

$$\langle n_f \rangle_{\vec{S}} = \sum_{i=1}^{\infty} \lambda_i \langle n_f \rangle_{r_i} \geq \sum_{i=1}^{\infty} \lambda_i \min(\langle n_f \rangle_{r_i}) = \min(\langle n_f \rangle_{r_i}), \tag{30}$$

where  $\lambda_i = P \left( \sum_{k=1}^{i-1} r_k < n_f \leq \sum_{k=1}^i r_k \right)$  and  $\sum_{i=1}^{\infty} \lambda_i = 1$  is used. Hence the mean of  $n_f$  with the waiting time (between restarts) sequence  $\vec{S}$  can be expressed as a convex combination of  $\{\langle n_f \rangle_{r_1}, \langle n_f \rangle_{r_2}, \langle n_f \rangle_{r_3}, \dots\}$ . Therefore, among general restart strategies, the mean hitting time with sharp restart always attains the lowest global minimum, as pointed out originally in Refs. [7, 16].

### Quantum renewal equation

Here we recap the first detected passage or first hitting statistics from the repeated-measurement protocol. The quantum renewal equation reads [54]

$$\varphi_n = \langle \delta | \hat{U}(n\tau) | 0 \rangle - \sum_{m=1}^{n-1} \langle \delta | \hat{U}[(n-m)\tau] | \delta \rangle \varphi_m. \tag{31}$$

$\varphi_n$  is the first-hitting amplitude whose squared absolute value gives the probability, namely  $F_n = |\varphi_n|^2$ . The unitary evolution between measurements gives  $\hat{U}(\tau) = \exp(-iH\tau)$  ( $\hbar$  is set as 1). Eq. (31) shows that the first-hitting amplitude is equal to the measurement-free transition amplitude  $\langle \delta | \hat{U}(n\tau) | 0 \rangle$  subtracting the measurement-free return amplitude  $\langle \delta | \hat{U}[(n-m)\tau] | \delta \rangle$  propagating from the prior first-hitting amplitude  $\varphi_m$  ( $m < n$ ). This is also the spirit of the classical renewal equation, with a replacement of the probability to amplitude [1]. One can in principal obtain all the  $\varphi_n$  from Eq. (31) by iterations, and then calculate  $F_n = |\varphi_n|^2$ , for all possible  $\delta$  and  $n$ . When  $|\delta\rangle = |0\rangle$ , i.e. the return case, we present a table of the first-hitting probability  $F_n$ , for the model of an infinite line considered in the main text, and this table is cited from Ref. [54], see Table I in the main text. For  $\delta = 10$ , we obtained Table II.

### A comparison between the results from two models

Here we will compare the results obtained from the non-Hermitian theory (NHT) with those from the repeated-measurement protocol (RMP), which was already recapped in last section. Without restart, The

TABLE II.  $F_n$  for the model of an infinite line,  $\delta = 10$ .

| $n$ | $F_n$  |
|-----|--|
| 1   | $ J_{10}(2\gamma\tau) ^2$  |
| 2   | $ J_0(2\gamma\tau)J_{10}(2\gamma\tau) - J_{10}(4\gamma\tau) ^2$  |
| 3   | $ J_{10}(2\gamma\tau)J_0^2(2\gamma\tau) - J_{10}(4\gamma\tau)J_0(2\gamma\tau) - J_0(4\gamma\tau)J_{10}(2\gamma\tau) + J_{10}(6\gamma\tau) ^2$  |
| 4   | $ J_{10}(2\gamma\tau)J_0^3(2\gamma\tau) - J_{10}(4\gamma\tau)J_0^2(2\gamma\tau) + J_{10}(6\gamma\tau)J_0(2\gamma\tau) - 2J_0(4\gamma\tau)J_{10}(2\gamma\tau)J_0(2\gamma\tau) + J_0(6\gamma\tau)J_{10}(2\gamma\tau) + J_0(4\gamma\tau)J_{10}(4\gamma\tau) - J_{10}(8\gamma\tau) ^2$ |

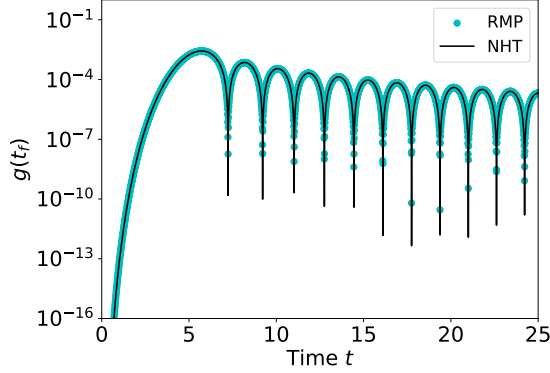


FIG. 6. The pdf of detection times as a function of time  $t$ , obtained from the non-Hermitian approximation Eq. (4) in the main text, compared with the first-hitting probability  $F_n$  in the time domain. For the latter, the data points  $(n\tau, F_n/\tau)$  are plotted. We chose  $\delta = 10$ , and  $\tau = 0.05$ .

probability density function (pdf) of detection times from NHT reads [Eq. (4) in the main text]

$$g(t_f) \sim \delta^2 \tau \frac{J_\delta^2(2t_f)}{t_f^2}. \quad (32)$$

And for the RMP, the pdf of detection times is actually  $g^{rm}(t_f) = \sum_{n=1}^{\infty} F_n \delta(t_f - n\tau)$  where  $rm$  means repeated measurements, with  $F_n = |\varphi_n|^2$  obtained from the quantum renewal equation [Eq. (31)]. When plotting the RMP results for comparison, to avoid the delta function, we will take the ‘‘local average’’  $(1/\tau) \int_{(n-1/2)\tau}^{(n+1/2)\tau} dt g^{rm}(t) = F_n/\tau$  [56]. See Fig. 6 where an excellent agreement between the two results is shown.

For the mean detection time under restart, Eq. (5) in the main text gives the formula derived from NHT, and with the RMP, the mean of  $n_f$  is

$$\langle n_f \rangle_r = \frac{1 - P_{\text{det}}(r)}{P_{\text{det}}(r)} r + \langle n_f \rangle_{\text{cond}}, \quad (33)$$

where  $\langle n_f \rangle_{\text{cond}} := \sum_{k=1}^r k F_k / \sum_{j=1}^r F_j$ . Substituting  $F_n$  into Eq. (33) gives the mean  $\langle n_f \rangle_r$  obtained from RMP. The comparison between the result from Eq. (5) in the main text and that from Eq. (33) evaluated numerically with the  $F_n$  found from the renewal equation, is presented

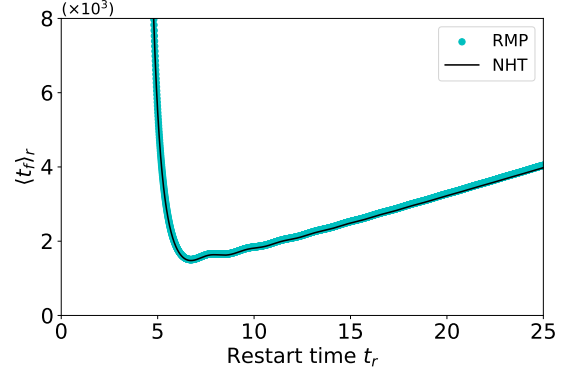


FIG. 7.  $\langle t_f \rangle_r$  vs. restart time  $t_r = r\tau$ . For  $\langle n_f \rangle_r$  calculated from the quantum renewal equation [Eq. (31)], the data points  $(r\tau, \tau \langle n_f \rangle_r)$  are plotted. The blue curve represents the non-Hermitian theory Eq. (5) in the main text. We used  $\delta = 10$ ,  $\tau = 0.01$ .

in Fig. 7. Clear the agreement is excellent for the small value  $\tau = 0.01$  under study.

#### An explicit expression of Eq. (5) in the main text

As shown in Eq. (5) in the main text, the integrals contain Bessel functions of the first kind  $J_\delta(2t_f)$  and powers of  $t_f$ . Further simplification gives

$$\langle t_f \rangle_r \sim [(\delta^2 \tau \mathcal{I}_1)^{-1} - 1] t_r + \mathcal{I}_2 / \mathcal{I}_1, \quad (34)$$

with

$$\begin{aligned} \mathcal{I}_1 &= \frac{1}{(4\delta^2 - 1)t_r} [(8t_r^2 + 2\delta + 1) J_\delta^2(2t_r) + 8t_r^2 J_{\delta+1}^2(2t_r) \\ &\quad - 4t_r(2\delta + 1) J_{\delta+1}(2t_r) J_\delta(2t_r)], \\ \mathcal{I}_2 &= t_r^{2\delta} \Gamma(2\delta) {}_2\tilde{F}_3(\delta, \delta + 1/2; \delta + 1, \delta + 1, 2\delta + 1; -4t_r^2), \end{aligned} \quad (35)$$

where  $\Gamma(x)$  is the gamma function, and  ${}_p\tilde{F}_q(a_1, \dots, a_p; b_1, \dots, b_q; z)$  is the regularized hypergeometric function, i.e.

$$\begin{aligned} &{}_2\tilde{F}_3(\delta, \delta + 1/2; \delta + 1, \delta + 1, 2\delta + 1; -4t_r^2) \\ &= \frac{{}_2F_3(\delta, \delta + 1/2; \delta + 1, \delta + 1, 2\delta + 1; -4t_r^2)}{\Gamma^2(\delta + 1)\Gamma(2\delta + 1)}, \end{aligned} \quad (36)$$

where  ${}_pF_q(a_1, \dots, a_p; b_1, \dots, b_q; z)$  is the hypergeometric function. With those results, the limits of  $\langle t_f \rangle_r$  in the main text are yielded.

#### Large $\delta$ case of Eq. (7) in the main text

Since  $F_n$  exhibits monotonical growth for small  $n$  and decays with superimposed oscillations when  $n > \delta/2\tau$

[55], the several minima of  $\langle t_f \rangle_r$  due to the oscillations appear when  $t_r > \delta/2$ . Hence in large  $\delta$  limit, the solutions to Eq. (7) in the main text,  $t_r^{ext} > \delta/2$  will be large. With the large argument approximation for  $J_\nu(x)$  and Eq. (35), Eq. (7) in the main text yields

$$\frac{1}{2}[1+(-1)^\delta] \sin(4t_r^{ext}) = 2(t_r^{ext}/\delta)^2 + (-1)^\delta (t_r^{ext}/\delta) \cos(4t_r^{ext}). \quad (37)$$

We note that solutions to Eq. (37) do not agree well with those to Eq. (7) in the main text, but the aim here is to provide an upper-bound for  $t_r^{ext}$ , which is feasible by analyzing Eq. (37). The left-hand side of Eq. (37) is bounded in  $[0, 1]$ , while the lower-bound of the right-hand side is  $2x^2 - x$  with  $x = t_r^{ext}/\delta$ . Thus the upper-bound of  $t_r^{ext}$  is given by  $2x^2 - x = 1$ , leading to  $t_r^{ext} < \delta$ . Namely, the minima of  $\langle t_f \rangle_r$  appear on the interval  $t_r \in [\delta/2, \delta]$ .

#### Details for $t_r$ vs. $\delta$

We present here the theoretical optimal restart time  $t_r$  as a function of  $\delta$  for  $\tau = 0.01$  and  $\tau = 0.05$ , and also compare the theory with the exact results. The theory is based on the minimization of  $\langle t_f \rangle_r$  from Eq. (5) in the main text, and the exact results are obtained from the repeated-measurement model, namely minimizing  $\langle n_f \rangle_r$  calculated with  $F_n$ . For the latter, we used  $t_r^* = r^* \tau$ . Fig. 8 shows the  $\tau$ -independence of  $t_r$ , as well as the non-trivial behavior of sudden jumps (as mentioned in the main text), which might be homologous to the plunges in large  $\tau$  limit. Fig. 9 shows the comparison between the theory and exact results for  $\tau = 0.01$ , and the case  $\tau = 0.05$  was also checked by the authors without showing here.

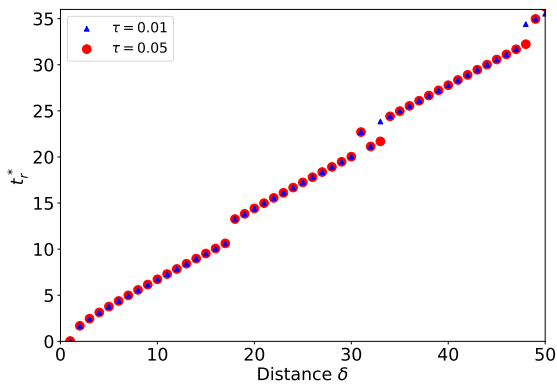


FIG. 8. The optimal restart time  $t_r$  versus  $\delta$  for  $\tau = 0.01, 0.05$ , obtained from the non-Hermitian theory. As shown,  $t_r$  increases roughly linearly in  $\delta$  due to the ballistic spreading of the quantum wave packet, and exhibits sudden jumps at some special  $\delta$ 's, which is speculated as being homologous to the plunges in large  $\tau$  limit.

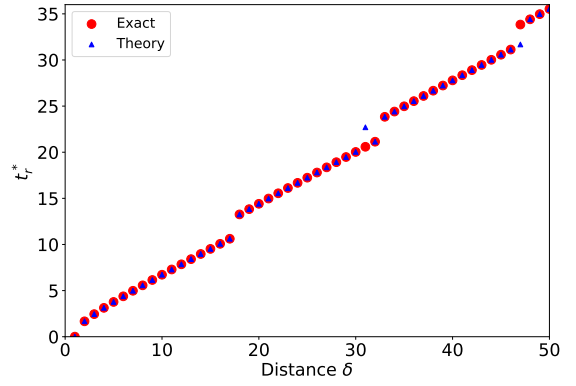


FIG. 9. The optimal restart time  $t_r$  versus  $\delta$  for  $\tau = 0.01$ . We compare the theoretical and exact results. The theory agrees with the exact results nicely, except on the blips.

#### The mean first hitting time under sharp restart for the classical model

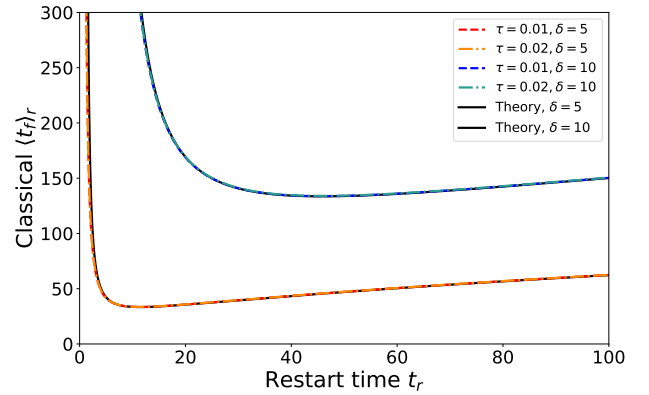


FIG. 10.  $\langle t_f \rangle_r$  vs.  $t_r$  for different  $\delta$  and  $\tau$ . The model here is a classical random walk in one dimension (as mentioned in the Introduction in the main text), and we employ the periodical monitoring again on this model to make a comparison with the quantum case. As seen, there is no counterpart of the quantum oscillations in the classical model. The black lines represent the theoretical convergence to a diffusion process under restart [Eq. (40)]. And the colored dashed curves represent the results obtained from the classical renewal equation [Eq. (38)] and Eq. (3) in the main text.

To make a comparison between the classical and quantum restart, we apply the sharp-restart strategy to a classical walk on the integers (the model mentioned in the Introduction in the main text) under periodical monitoring. More specifically, the random walk is started on the origin, and the detection is on lattice point  $\delta$ . Every  $\tau$  units of time, the experimentalist measures if the particle is on  $\delta$  or not (thus we are dealing with a problem of first detection and not first passage like in the quantum setting). Restarts are sharp and take place every  $r$  units

of time. To summarize the detection protocol is exactly like the one introduced in the main text for the quantum particle, but the dynamics between measurements is classical.

As for the quantum case studied in the Letter we focus on the small and large  $\tau$  limit. When  $\tau$  is large, such that  $\delta^2/D$  is much smaller than  $\tau$ , where  $D$  is the diffusion constant, i.e.  $D = 1$  in our case (with the hopping rate  $\gamma$  set as 1), we expect simple behavior. Namely that the most efficient restart is found for  $r = 1$ . Simply stated, as the packet is spreading for large  $\tau$ , it is better to speed up the restarts. Mathematically, this is related to the observation that the classical first hitting probability  $F_n^{\text{cl}}(\delta)$  in this limit is a monotonically decaying function of  $n$ . The significance of this, is that the staircases found for large  $\tau$ , in the quantum world (see Fig. 3 in the main text) will not be found for the classical case.

We now focus on small  $\tau$  limit of the classical restart. Unlike the quantum case, the classical counterpart does not suffer from the Zeno physics. Let us focus on the general formalism of this problem, valid for any  $\tau$ . The first thing to do is to calculate  $F_n^{\text{cl}}(\delta)$  the first hitting probability, in the classical domain. Using the solution mentioned in the main text, that the probability of finding the classical walker on  $x$  at time  $t$  is  $P^{\text{cl}}(x, t) = i^{-x} e^{-2\gamma t} J_x(i2\gamma t)$ , and the classical renewal equation

$$F_n^{\text{cl}}(\delta) = P^{\text{cl}}(\delta, n\tau) - \sum_{m=1}^{n-1} P^{\text{cl}}[0, (n-m)\tau] F_m^{\text{cl}}(\delta), \quad (38)$$

one can readily obtain the first hitting statistics. Using those  $F_n^{\text{cl}}(\delta)$ , with the general formula Eq. (3) in the main text, the mean hitting time under sharp restart and discrete sampling can be calculated for example numerically. As seen in Fig. 10, for small  $\tau$ , the mean hitting time under sharp restart exhibits one distinct minimum and smooth landscape without oscillations. Hence, the oscillations in Fig. 3 in the main text (which focus on small  $\tau$  limit) have no counterpart in the classical model.

Let us analyze the small  $\tau$  limit more carefully. What is expected is the  $\tau$ -independence of  $\langle t_f \rangle_r$  in the small  $\tau$  limit, since the dynamics of a classical random walk under discrete monitoring converges to a diffusion process, i.e. Brownian motion. The classical first passage probability for a diffusive walker is known as the Smirnov distribution [1]

$$f^{\text{cl}}(\delta, t) = \frac{\delta}{\sqrt{4\pi Dt^3}} e^{-\delta^2/4Dt}. \quad (39)$$

As mentioned, with the hopping rate  $\gamma$  in Eq. (1) in the text set as 1, the diffusion coefficient  $D = 1$ . And the

continuous time limit of Eq. (3) in the main text gives

$$\begin{aligned} \langle t_f \rangle_r &= t_r(1 - I_1)/I_1 + I_2/I_1 \\ \text{with } I_1 &= \text{erfc}\left(\frac{\delta}{2\sqrt{t_r}}\right), \\ I_2 &= \frac{\delta\sqrt{t_r} e^{-\delta^2/4t_r}}{\sqrt{\pi}} - \frac{\delta^2}{2} \text{erfc}\left(\frac{\delta}{2\sqrt{t_r}}\right), \end{aligned} \quad (40)$$

where  $\text{erfc}(x) = 1 - \text{erf}(x)$  is the complementary error function, with  $\text{erf}(x)$  the error function. Eq. (40) gives the theoretical results shown in Fig. 10, which reach excellent agreement with the numerics calculated from Eq. (38). The analysis in this section while focusing on small and large  $\tau$  limits, will be extended elsewhere.

### Derivation of Eq. (10) in the main text

Substituting the expression of  $F_n$  into Eq. (9) in the main text, we get

$$\sum_{n=1}^r \frac{1}{n} \cos^2\left(2n\epsilon - \frac{\pi}{4}\right) = \frac{r}{r+1} \cos^2\left[2(r+1)\epsilon - \frac{\pi}{4}\right], \quad (41)$$

where  $\epsilon$  is defined as in the main text,  $\tau = k\pi/2 + \epsilon$  with  $0 < \epsilon < \pi/2$ . The  $\epsilon$  solving Eq. (41) gives the special  $\epsilon$  at which the transition from  $r^* = r$  to  $r^* = r+1$  takes place. As mentioned if  $\epsilon = 0$ ,  $r^* = 1$ . We denote  $\epsilon_{1 \rightarrow 2}$  as the value of  $\epsilon$  where we have a transition from  $r^* = 1$  to  $r^* = 2$ , similarly for other transitions. In between the transition  $\epsilon$ , namely for each interval  $[\epsilon_{k \rightarrow k+1}, \epsilon_{k+1 \rightarrow k+2}]$ , we will check whether  $\langle n_f \rangle_{k+1}$  remains the minimum, and especially compare it with  $\langle n_f \rangle_1$  in case we miss the plunge to  $r^* = 1$ . We get the following:

$$\begin{aligned} \epsilon_{1 \rightarrow 2} &= 0.850, \\ \epsilon \in [\epsilon_{1 \rightarrow 2}, \epsilon_{2 \rightarrow 3}] &: \langle n_f \rangle_2 < \langle n_f \rangle_1, \\ \epsilon_{2 \rightarrow 3} &= 1.081, \\ \epsilon \in [\epsilon_{2 \rightarrow 3}, \epsilon_{3 \rightarrow 4}] &: \langle n_f \rangle_3 < \langle n_f \rangle_1, \\ \epsilon_{3 \rightarrow 4} &= 1.204, \\ \epsilon \in [\epsilon_{3 \rightarrow 4}, \epsilon_{4 \rightarrow 5}] &: \langle n_f \rangle_4 < \langle n_f \rangle_1, \\ \epsilon_{4 \rightarrow 5} &= 1.280, \\ \epsilon \in [\epsilon_{4 \rightarrow 5}, \epsilon_{5 \rightarrow 6}] &: \langle n_f \rangle_5 < \langle n_f \rangle_1, \\ \epsilon_{5 \rightarrow 6} &= 1.332, \\ \epsilon \in [\epsilon_{5 \rightarrow 6}, 1.353] &: \langle n_f \rangle_6 < \langle n_f \rangle_1; \\ \epsilon \in [1.353, \pi/2] &: \langle n_f \rangle_1 < \langle n_f \rangle_6. \end{aligned} \quad (42)$$

We note that Eq. (41) gives more than one solutions for given  $r$ . For instance, for  $r = 1$ , the solutions are 0.850 and 1.293, and a careful check on  $\langle n_f \rangle_r$  excludes 1.293 since  $r^* = 5$  at this  $\epsilon$ . Eq. (10) in the main text is obtained then.



$r^*$  for the case  $\delta = 0$  on the full range of  $\tau$

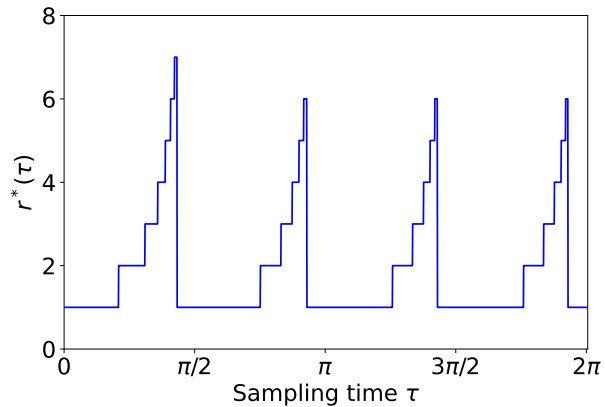


FIG. 11. The optimal restart time  $r^*$  as a function of  $\tau$  for  $\delta = 0$ . We see the staircase structure appears when  $\tau$  is not large.

As mentioned, for large sampling time  $\tau$ , the optimal restart step  $r^*$  as a function of  $\tau$  exhibits staircase structure presented in Fig. 3 in the main text. Actually, for the return case  $\delta = 0$ , the staircase structure appears on the full range of  $\tau$ . We show in Fig. 11 the  $r^*$  versus  $\tau$  with  $\tau \in [0, 2\pi]$ . The staircase composed by  $r^* = 1, 2, \dots, 5, 6$  starts from  $\pi/2$ , and before that is a staircase composed by  $r^* = 1, 2, \dots, 5, 6, 7$ .